Journal of Power Sources 267 (2014) 323–328

Contents lists available at ScienceDirect

Journal of Power Sources

journal homepage: www.elsevier.com/locate/jpowsour

Influence of thermal post-curing on the degradation of a cross-linked polybenzimidazole-based membrane for high temperature polymer electrolyte membrane fuel cells

T. Ossiander [a], M. Perchthaler [b], C. Heinzl [a], C. Scheu [a, *]

[a] Department of Chemistry, Ludwig-Maximilians-University Munich, Butenandtstr. 11, 81377 Munich, Germany
[b] Graz University of Technology, Institute of Chemical Engineering and Environmental Technology, Steyrergasse 21, 8010 Graz, Austria

HIGHLIGHTS

- Thermal post-curing of cross-linked polybenzimidazole-based HTPEM under air.
- Post-cured membranes showed higher mechanical, thermal and chemical *ex-situ* stability.
- Durability in fuel cell cycled operation was improved by longer post-curing times.
- The occurring degradation mechanisms were determined.
- Longer post-curing period were shown to enhance the resistance against short circuits.

ARTICLE INFO

Article history:
Received 7 November 2013
Received in revised form
11 April 2014
Accepted 29 April 2014
Available online 28 May 2014

Keywords:
High temperature polymer electrolyte membrane
Fuel cell
Polybenzimidazole
Thermal post-curing
Degradation mechanisms

ABSTRACT

The lifetime stability of membranes is one of the main requirements regarding reliability of high temperature polymer electrolyte membrane fuel cells. The present work has improved durability under cycled operation by thermal post-curing of cross-linked polybenzimidazole (PBI)-based membranes. The membranes were dried over 1, 2 and 3 h at 250 °C under air. Ex-situ experiments proved an increase in stability by post-curing. The liquid uptake and swelling in phosphoric acid increased with longer curing periods. The effect of thermal treatments on cycle stability, lifetime and begin-of-life performance of the membrane electrode assemblies (MEAs) was investigated. Longer post-curing periods of the membranes had no influence on the MEAs' begin-of-life performance and constant current behavior over 2300 h. However, the 3 h post-cured MEAs showed enhanced cycle stability. *Post-mortem* analysis was carried out to identify the occurring degradation mechanisms. While a significant loss of phosphoric acid and a reduction of electrochemical surface activity on the cathode were observed for both post-cured MEAs, the 3 h dried membrane sample had a significantly higher resistance against pinhole formation during the long term test. Altogether, this work presents thermal post-curing as a promising method for the reduction of degradation determining effects in fuel cell membranes.

1. Introduction

Within the last years of fuel cell development major attention was given to polymer electrolyte membrane fuel cells because of their promising high efficiency. This technology is often based on perfluorosulfonic acid polymer membranes (e.g. Nafion®) [1]. As the proton conductivity in these membranes is dependent on presence of liquid water, their operation temperature has to be lower than 100 °C. This results in two main limitations. First, a humidification of the reactant gas is required in order to keep the conductivity high enough for fuel cell applications. Second, the catalyst is more sensitive against impurities, especially carbon monoxide, at temperatures less than 100 °C [2,3].

High temperature polymer electrolyte membranes (HTPEM) using phosphoric acid doped polybenzimidazole (PBI) as proton conductor operate at higher working temperatures of 150–200 °C without the necessity of humidification of the reactant gases [4–6]. These temperatures have additional benefits such as faster reaction kinetics on the electrodes, increased catalytic activity and simplified heat management [7–10].

In spite of these advantages, the lifetime of the HTPEM membrane electrode assemblies still remains the major concern. Several achievements have been made in the last years for constant current

* Corresponding author. Tel.: +49 89 2180 77184; fax: +49 89 2180 77622.
E-mail address: Christina.Scheu@cup.uni-muenchen.de (C. Scheu).

http://dx.doi.org/10.1016/j.jpowsour.2014.04.158
0378-7753/

measurements [11,12]. However, the goal of minimal performance losses over long operating periods with a large number of shut downs, remains challenging [13]. In several studies, the lifetime reducing degradation effects have been investigated [11,12,14–16]. However, the detailed mechanisms that occur in the different MEA components and the relative contribution of each material's degradation are not yet completely understood [17].

For HTPEM fuel cells a higher resistant membrane against chemicals, heat and mechanical stress in combination with an enhanced level of proton conductivity is essential [17,18]. Therefore, new membranes should not only show improved stability but also allow a higher phosphoric acid binding capacity [19]. Striving for the goals of performance, lifetime and cost on the membrane side, different approaches have been reported in literature [17–20]. Most of these concepts rely on new combinations of polymers and their additives. In order to build strong covalent linkages with the imidazole groups of the PBI, covalent cross-linkers are in use. The cross-linked PBI has a higher stability than membranes of pure PBI. Various different cross-linkers are in use, such as organic diacids [21], dihalides [22–25], diisocyanates [26,27] and diepoxides [28–30]. Wang et al. reached a better mechanical and chemical stability same as a higher conductivity at higher phosphoric acid doping levels of an epoxy cross-linked PBI membrane [30]. Lin et al. improved the performance of a PBI membrane by producing mechanical stable, cross-linked membranes with lower thicknesses and therefore reduced electrolyte resistance [31]. Aside from these material variations, the fabrication and post-treatment parameters were found to have large influences on the properties of the final membrane [18,32,33]. During membrane formation, the duration and temperature of various drying steps influence the materials' morphology [33–35]. It was found that thermal treatment did positively influence the liquid uptake behavior and acid binding capacity as well as the lifetime and cycle stability [36–38]. Due to thermal post-curing of a pure PBI membrane for 16 h at 350 °C under argon, Aili et al. achieved higher lifetime under constant operation at 0.6 A cm^{-2} [33].

In the present work, the influence of shorter thermal post-treatment under air at 250 °C on PBI-based membranes is analyzed. Systematic examinations of the mechanical, thermal and chemical properties are carried out and the data are compared to electrochemical lifetime behavior of the MEAs under start-stop cycling and 2300 h constant operation. An understanding of the occurring degradation mechanisms of the different samples should give a deeper insight in the benefits of membrane post-curing.

2. Experimental

2.1. Membrane preparation

The membranes were solution casted from dimethylacetamide (DMAc, synthesis grade, Merck). Therefore, *meta*-PBI powder was dissolved in DMAc under stirring for 3 h at 200 °C under pressure. A solution of bisphenol A diglycidyl ether (synthesis grade, Sigma Aldrich) in DMAc was added. All chemicals were used as purchased without further purification. The membranes were casted by solvent evaporation at 70–100 °C on a carrier foil. Thermal post-treatment in the dryer was done for 1, 2 and 3 h at 250 °C under air. Membranes with longer post-treatment got brittle and were therefore not tested in this work. The cross-linked membranes were referred to as M0 (0 h), M1 (1 h), M2 (2 h) and M3 (3 h). The average thickness variation of the sheets was below 1 μm.

2.2. Ex-situ membrane characterization

The thermal stabilities of the membrane samples were determined by thermo gravimetric analysis (TGA) on a *Perkin–Elmer TGA 4000*. About 10 mg of the material were filled into the crucible. All measurements were recorded with a heating rate of 10 °C min^{-1} and under nitrogen atmosphere.

The solubility of the membranes was tested by extraction in DMAc. Pieces in the size of 3 cm × 3 cm were dried in the oven over night at 150 °C before their weight was measured. After this, the membrane was put into a round bottom flask and covered with DMAc. The solvent was heated up to 130 °C for one hour. After cooling the solution to room temperature, the extracted samples were dried over night at 150 °C and weighted afterwards. The extraction residue was calculated as the remaining percentage of the membranes' mass.

The swelling behavior and liquid uptake of the membranes were determined by immersing 2.5 cm × 3 cm pieces in phosphoric acid for 30 min at 130 °C. The weight and dimensional changes between the dry and the doped membrane were recorded. Liquid uptake and swelling ratios were calculated as percentage weight increase and dimensional growth.

The mechanical properties of the samples were determined by measuring stress–strain curves on a *BT1 FR0.5TN.D14/500 N Zwicki* from *Zwick*. Membrane pieces (1 cm × 15 cm) were punched out of the membrane. The average thickness of every sample was evaluated with a thickness gauche from *Sylvac*. All measurements were carried out at room temperature.

To investigate a possible change of crystallinity in the membranes, X-ray diffraction (XRD) patterns were taken on a Seifert THETA/THETA-diffractometer (GE Inspection Technologies) equipped with a Meteor OD detector, using Co-K_α radiation ($\lambda = 1.79$ Å). A 2θ detection range of 10–70°, a step size of $2\theta = 0.05°$ and an acquisition time of 10 s/(2θ-step) were used.

2.3. MEA preparation

The catalyst support (high surface area carbon, HSAC, BET: 250–300 m^2 g^{-1}) material with PTFE as hydrophobic binder material was applied on a wet proofed carbon based gas diffusion layer from Freudenberg Fuel Cell Technologies (FFCT) via a doctor blade process. The height of the doctor blade was adjusted to 610 μm to get an optimal loading of carbon/PTFE on the gas diffusion layer and dried at 170 °C under constant air flow. The platinum catalysts were deposited on the catalyst support layer via an electroless deposition method by impregnating a solution of H_2PtCl_6 into the catalyst support layer with subsequent thermal reduction. The platinum to carbon ratio was set to 0.4. The obtained crystallite size of the platinum particles on the HSAC was 2.7 nm, which was determined by XRD measurements. The MEAs were then manufactured by doping the catalyst layer with phosphoric acid and hot pressing them with the membrane. All samples had the same amount of phosphoric acid in the finally obtained MEA.

2.4. MEA-testing

The begin-of-life (BOL) polarization curves were determined in a single cell setup with an active area of 50 cm^2 and a single serpentine channel flow field structure on anode and cathode. Reactant flow rates were measured and controlled using mass flow controllers. The cell temperature was set to 160 °C controlled by electrical heating cartridges and the gas stoichiometry was kept constant at 1.2 for hydrogen and 2.0 for air.

Start stop cycle tests were done to investigate the stability of the MEAs under fuel cell cycling operation. A 50 cm^2 single cell was heated up to 80 °C. At this temperature, the cathode was purged with dry air for five minutes. Then the cell was heated to 120 °C. At this temperature, the anode was purged with nitrogen. Afterwards the hydrogen flow on the anode and the air flow on the cathode

were switched on. While the cell was heated up to 160 °C, current was drawn at 0.25 A cm^{-2}. As soon as 160 °C was reached, the current was increased to 0.5 A cm^{-2} and then held for 4 h. In the stop period, the current was decreased to 0.25 A cm^{-2} while cooling the cell to 120 °C. The current was switched off when this temperature was reached. Afterwards, the anode was purged with nitrogen and the cell cooled down to room temperature for four hours. This procedure was repeated for 28 cycles.

Long term operation under constant load was conducted at a current density of 0.2 A cm^{-2} at 160 °C. The stack with MEAs with an active area of 153 cm^2 was fueled with reformed methanol (77 vol% H_2, 1 vol% CO and 22 vol% CO_2) on the anode with a stoichiometry of 1.4 and air at the cathode with a stoichiometry of 2.0.

2.5. Exhaust gas analysis

The exhaust gas of the cathode and of the anode was collected with a condensation trap, which cools the exhaust gas streams down to a dew point of 2 °C. The collected water from the anode and from cathode gas exhaust stream was separately collected and the H_3PO_4 content was determined by the reaction of H_3PO_4 with molybdenum blue in a UV/VIS spectrometer *Lambda 35* from *Perkin Elmer*.

2.6. MEA post-mortem analysis

The catalytic active surface area of the samples was determined from cyclic voltammograms using a *Zahner PP241* (Zahner Elektrik) and a *Zahner IM6ex* electrochemical workstation. The MEAs were tested in a 153 cm^2 single cell and fed with dry hydrogen on the anode and humidified nitrogen on the cathode. The electrochemical surface area (ECA) was determined by cycling the cathode between 0.095 and 1.1 V with 0.1 V s^{-1} 100 times, followed by an analysis scan with 0.05 V s^{-1}. The ECA was calculated according to Equation (1).

$$\mathrm{ECA}\left(\mathrm{cm^2 mg^{-1}}\right) = \mathrm{Charge}\left(\mu\mathrm{C\,cm^{-2}}\right) \Big/ \left[210\left(\mu\mathrm{C\,cm^{-2}}\right) \times \text{catalyst loading}\left(\mathrm{mg\,cm^{-2}}\right)\right] \quad (1)$$

To obtain the acid content of the MEAs before and after operation, they were extracted in water at 70 °C over night. The acid content in the resulting extract was analyzed by the intensity of molybdenum blue reaction in a UV/VIS spectrometer *Lambda 35* from *Perkin Elmer*.

Electrical short circuits in the active area of the MEAs after operation were located with an infrared camera from *Fluke* by detection of the hot spots under voltage.

3. Results and discussion

3.1. Thermal stability

The influence of post-curing on the samples' thermal stabilities between 40 and 600 °C is shown in Fig. 1. A first mass loss that is due to the evaporation of around 6 wgt-% water and traces of DMAc appears in all measurements. When heating the samples further, first differences occur in the temperature range between 150 °C and 250 °C, when the undried material looses 3.9 wgt-%, whereas the mass of the other samples remain nearly unchanged. With the boiling point of DMAc being at 165 °C, these results indicate a complete evaporation of loose bound DMAc during post-treatment. In the temperature range between 250 and 350 °C the weight loss of all samples is different (Fig. 1). Whereas the undried material evaporates 10.5 wgt-%, the 3 h dried membrane had a loss of

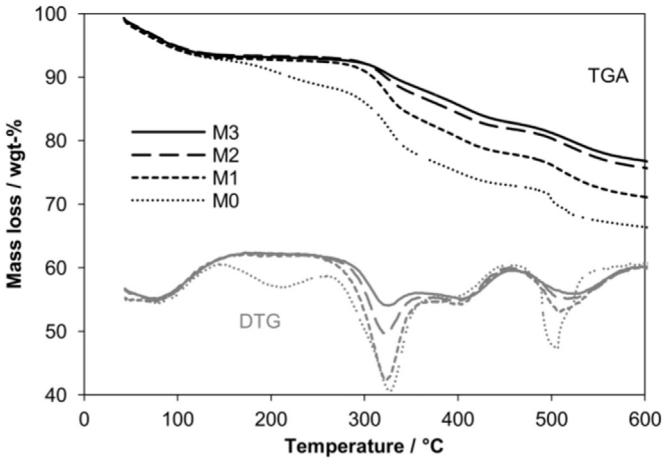

Fig. 1. TGA-comparison of four different drying periods while heating the material up to 600 °C.

5.6 wgt-%. In this temperature range the stronger bound DMAc is decomposing. The glass transition point of pure PBI films casted from DMAc is known to be around 400 °C and the decomposition starts at temperatures above 600 °C [35,39]. The structural changes in the PBI are reported to begin above 350 °C [33–35]. Therefore, the identical weight losses above 350 °C are not discussed here. Overall, 1 h post-curing resulted in a higher thermal stability in a temperature range till 300 °C compared to the undried membrane by containing less DMAc, whereas a thermal post-treatment of 3 h reduced the decomposition of the membrane samples even at higher temperatures. These results are in correlation with the data reported from Aili et al. for post-cured, pure PBI-membranes [33].

3.2. Dimensional changes

The experimental data in Table 1 summarize the dimensional and color changes after different post-curing periods. Every additional hour of drying leads to shrinking of the membrane both in plane and in thickness. When the solvent DMAc evaporates out of the material and the polymer is thermally treated for a long period, the dynamics of the polymer chains raise. Due to this the probability that they can relax into their initial structure increases and it can be speculated that the polymer chains start to coil. This behavior is often found for heat treated polymer films [40]. This dense structure freezes in when cooling the samples under air directly to room temperature, leading to smaller dimensions. The color of the membranes got darker during post treatment, which indicates morphological changes. Color changes are often observed when the polymer chains align in preferred direction or the amount of amorphous or crystalline phase increases [41]. The XRD data of the samples M0 to M3 are shown in Fig. 2. In all patterns a broad peak with a maximum at around 22° 2θ is observed which indicates a predominantly amorphous character of the PBI, which is also often found in literature [34]. For the membrane M0 two distinct

Table 1
Dimensional and optical changes at different post-curing periods.

Drying period [h]	Shrinking in plane [%]	Shrinking in thickness [%]	Color
0	–	–	Yellow
1	6.6	5.9	Lightbrown
2	7.4	6.6	Brown
3	12.1	8.8	Darkbrown

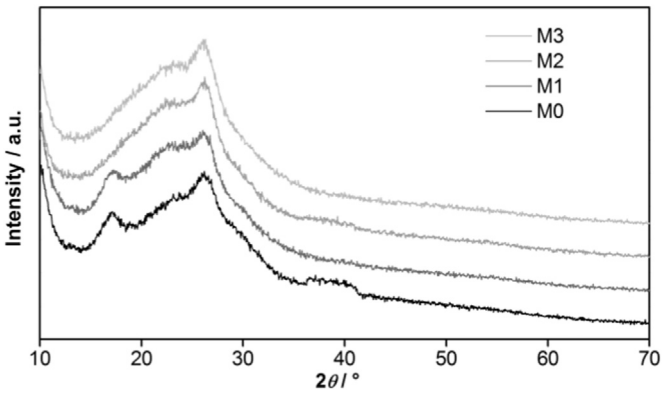

Fig. 2. X-ray diffraction patterns of all investigated membrane M0, M1, M2 and M3.

peaks occur in addition at 17.1° and 26.0° 2θ values which can be correlated to a partially crystalline character of the membrane. The 2θ values correspond to periodicity lengths of 6.0 Å and 4.0 Å respectively. While the signal at 26.0° does not change with increased heating time, the signal at 17.1° exhibits reduced intensity after one hour of heat treatment (membrane M1) and disappears after two or more hours (membrane M2 and M3). This leads to the assumption that due to the heating the larger ordered structures in the membrane decrease whereas the crystalline parts responsible for the peak at a scattering angle of 26.0° are not affected. Thus, we assume that the darkening is attributed to a change in crystallinity as well as a higher density, resulting from membrane shrinking.

3.3. Solubility in DMAc, liquid uptake and swelling

The solubility of different post-cured samples in DMAc are shown in Fig. 3. The extraction residues rise with the curing period. The highest insolubility is observed for the 3 h treated material with a residue of 89%, whereas the not cured membrane dissolves completely in DMAc. These results are also in agreement with the results of Aili et al. for post-cured, pure PBI-membranes [33]. Therefore, the main benefit for the enhanced stability against solubility in DMAc is gained from the structural changes within the polymer membrane and not by additional cross-linking effects. The liquid uptake of the samples in phosphoric acid is increased linearly from 360 to 820% by extending the curing period from 0 h to 3 h. Whereas the swelling of the membranes in plane also showed a linear increase, the swelling in thickness is reduced by longer post-curing periods. Longer thermal treatment enhanced the liquid uptake and swelling of the samples, while keeping the flexibility and handling properties of the doped membranes. Due to the added cross-linker, the undried samples did not dissolve in the acid, which is in concordance with the literature data [30,33].

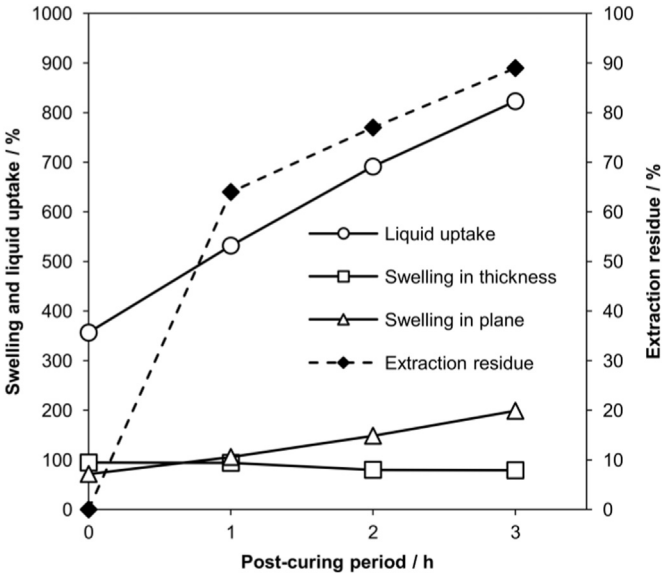

Fig. 3. Extraction residues in DMAc same as liquid uptakes and swelling in phosphoric acid of different post-cured samples.

3.4. Mechanical stability

Stress-strain curves of the different post-cured materials were measured to test the mechanical stability of the samples (Fig. 4). Within the first hour of drying the largest change in microstructure occurs, leading to improved mechanical properties. The Young's modulus rises from an average of 3.6–4.7 GPa and the yield stress increases from 110 to 160 MPa. With further post-curing an improved yield and ultimate stress was observed. On the other hand, additional drying reduced the ultimate strain from 50% to a minimum of 13%. Therefore, post-curing enhanced the strength in the elastic region and reduced the plastic deformation. This is in agreement with the results recently reported for phosphoric acid doped PBI-membranes at higher curing times and temperatures [33].

3.5. Polarization curves

The polarization curves in Fig. 5 reveal just a minor influence of post-treatment on the MEAs' performance. Therefore, the structural changes that were observed *ex-situ* for the membranes with 3 h post-curing data do not result in a higher BOL performance. As all three samples are equivalent in BOL performance, only the 1 h and 3 h dried samples were further analyzed regarding lifetime stability.

3.6. Constant current operation and start-stop-cycles

In constant fuel cell operation, the MEAs of the cross-linked membrane show significantly better performance and durability in comparison to the 3 h dried PBI reference membrane (Fig. 6). On the other side, at a current density of 0.2 A cm^{-2}, the post-treatment of the membranes has no influence on the degradation rate of the MEA. The break between 1700 and 1900 h can be attributed to a 200 h fuel cell test station shutdown.

The cycle stability of the 1 h and 3 h post-cured membranes was simulated in MEAs under fuel cell conditions via start-stop cycling at 0.5 A cm^{-2}. The results are shown in Fig. 7. The graph

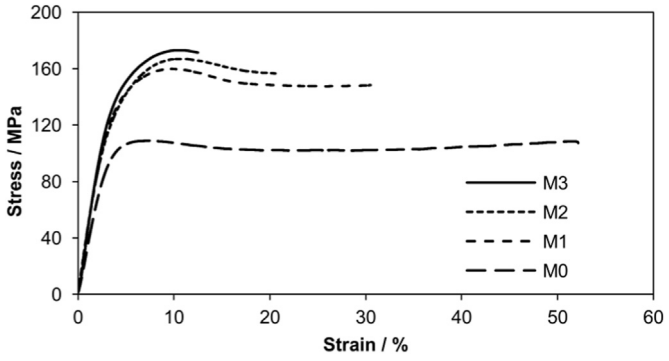

Fig. 4. Stress–strain-curves of different post-cured membrane samples.

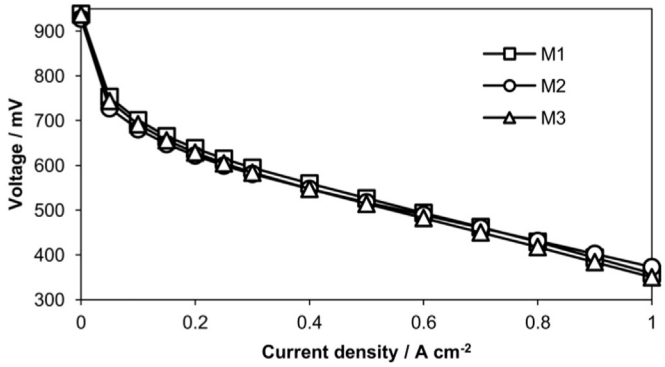

Fig. 5. Polarization curves of the post-cured membrane samples.

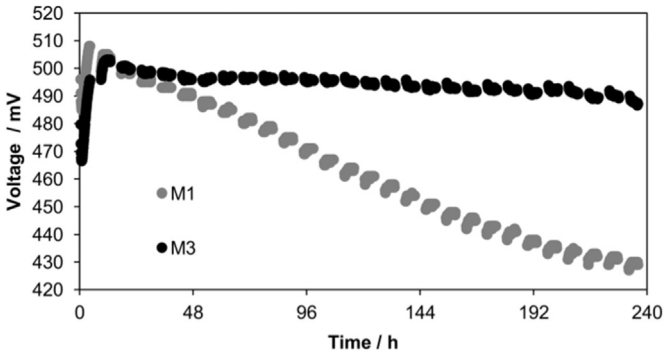

Fig. 7. Start-stop cycling of 1 h and 3 h post-cured membranes. For clarity only constant operation at 0.5 A cm^{-2} is plotted in the graph.

demonstrates that the degradation rate per cycle of the 3 h dried material is lower compared to the 1 h dried material. At lower current densities of 0.2 A cm^{-2} the post-treatment of the membranes has no influence on the degradation rate, whereas the longer dried samples show a significant lower degradation rate at the higher current densities during start-stop cycling. These current density depending results correlate with the data published for higher temperatures under argon treatment [33]. Therefore, the measured data prove that lower post-treatment temperatures and shorter drying times of 3 h at 250 °C under air result in the same benefits as 16 h thermal treatment at 350 °C under argon. In addition to that, the positive effect of thermal post-treatment can also improve the lifetime of a cross-linked membrane.

3.7. Degradation analysis

Looking at the common degradation mechanisms in fuel cell membranes, the following lifetime determining effects can explain the higher cycle stability of longer post-cured materials. The cathode ECA of the samples before and after operation was measured by cyclic voltammetry on the cathodes. The ECA of the 1 h post-cured sample was reduced by 27% from 120 to 88 $cm^2\ mg^{-1}$. In comparison to a 20% loss from 120 to 96 $cm^2\ mg^{-1}$ of the MEA with the 3 h dried membrane, the difference of 7% is not high enough for being the main mechanism resulting in such a high degradation rate. Another effect that is often observed in HTPEM-MEAs is the loss of phosphoric acid [42,43]. The determination of the phosphoric acid content in the exhaust gases and extraction of the MEAs after start-stop operation indicate that a significant amount of phosphoric acid is washed out. All MEAs lost around 36 wgt-% of phosphoric acid in total with a steady phosphoric acid loss of 2.7 μg h^{-1} into the exhaust gases. However, as the leaching is independent of the post-curing period of the membrane, it is not the major effect in this case. To analyze the formation of pinholes or fractures in the membrane during MEA operation, electrical short circuit localization tests were carried out. Observation of the start-stop-cycled MEAs revealed that the 1 h dried samples formed short circuits in the active area of the MEA, whereas the 3 h cured materials still possessed good performance and no short circuits could be observed. Therefore, thermal curing enhances the resistance of the membrane material against short circuit formation and leads to a lower degradation rate at higher current densities under cycled operation.

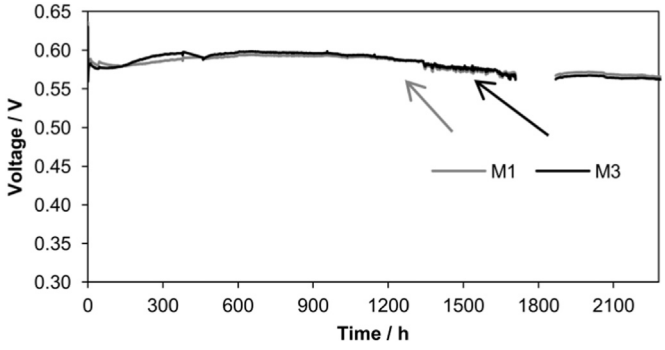

Fig. 6. Constant current measurements at 0.2 A cm^{-2} of the MEAs of M1, M3 and P3 membranes.

4. Conclusion

In order to investigate the influence of thermal post-curing on cross-linked membranes, they were treated for 1, 2 and 3 h at 250 °C under air in the oven. *Ex-situ* experiments proved an increase in mechanical and thermal stability and higher stability in solvents of the thermally treated membranes. A higher acid uptake capacity and chemical linkage were observed such as a better thermal resistance and higher strength of the material. The effect of different thermal post-curing on BOL performance, degradation under constant load and start-stop-cycling stability of a PBI-based fuel cell membrane was investigated. In BOL polarization curves the samples were shown to be unaffected by different curing times. The degradation rate at a current density of 0.2 A cm^{-2} under constant operation also did not change by rising the curing period from 1 to 3 h. Otherwise, a high influence of post-curing was observed under start-stop-cycled operation at 0.5 A cm^{-2}. After 3 h post-curing a significant reduced degradation and better cycle stability of the MEAs at the same level of BOL performance was observed. *Post-mortem* analysis of the MEAs revealed three degradation mechanisms of reduced cathode catalyst activity, acid loss and pinhole formation. Resulting in short circuits, pinhole formation was found to be the reason for the higher degradation rate of 1 h post-cured MEAs. Overall, the present work shows that 3 h post-curing of cross-linked membranes at 250 °C under air significantly enhances the MEAs' resistance against short circuits. Therefore, post-curing under air is presented as a promising method for the reduction of degradation determining effects.

Acknowledgments

Financial support from the German Federal Ministry for Economy and Technology is gratefully acknowledged. The authors thank Benjamin Breitbach and Stephan Gleich, Max-Planck-Institute for Iron Research, Düsseldorf, for support on the XRD measurements.

References

[1] J.A. Asensio, E.M. Sánchez, P. Gómez-Romero, Chem. Soc. Rev. 39 (2010) 3210.
[2] Q. Li, H.A. Hjuler, N.J. Bjerrum, Electrochim. Acta 45 (2000) 4219–4226.
[3] S. Gottesfeld, T.A. Zawodzinski, in: Advances in Electrochemical Science and Engineering, Wiley-VCH Verlag GmbH, 2008, pp. 195–301.
[4] Q. Li, J.O. Jensen, R.F. Savinell, N.J. Bjerrum, Prog. Polym. Sci. 34 (2009) 449–477.
[5] Q. Li, R. He, J.O. Jensen, N.J. Bjerrum, Chem. Mater. 15 (2003) 4896–4915.
[6] O. Savadogo, J. Power Sources 127 (2004) 135–161.
[7] S.K. Zecevic, J.S. Wainright, M.H. Litt, S.L. Gojkovic, R.F. Savinell, J. Electrochem. Soc. 144 (1997) 2973–2982.
[8] Y.-L. Ma, J.S. Wainright, M.H. Litt, R.F. Savinell, J. Electrochem. Soc. 151 (2004) A8–A16.
[9] C.-P. Wang, H.-S. Chu, Y.-Y. Yan, K.-L. Hsueh, J. Power Sources 170 (2007) 235–241.
[10] A.R. Korsgaard, R. Refshauge, M.P. Nielsen, M. Bang, S.K. Kær, J. Power Sources 162 (2006) 239–245.
[11] Y. Oono, A. Sounai, M. Hori, J. Power Sources 210 (2012) 366–373.
[12] T.J. Schmidt, ECS Trans. 1 (2006) 19–31.
[13] C. Hartnig, T.J. Schmidt, J. Power Sources 196 (2011) 5564–5572.
[14] J. Yu, T. Matsuura, Y. Yoshikawa, M. Nazrul Islam, M. Hori, Phys. Chem. Chem. Phys. 7 (2005) 373–378.
[15] A.D. Modestov, M.R. Tarasevich, V.Y. Filimonov, N.M. Zagudaeva, Electrochim. Acta 54 (2009) 7121–7127.
[16] Y. Oono, A. Sounai, M. Hori, J. Power Sources 189 (2009) 943–949.
[17] R. Borup, J. Meyers, B. Pivovar, Y.S. Kim, R. Mukundan, N. Garland, D. Myers, M. Wilson, F. Garzon, D. Wood, P. Zelenay, K. More, K. Stroh, T. Zawodzinski, J. Boncella, J.E. McGrath, M. Inaba, K. Miyatake, M. Hori, K. Ota, Z. Ogumi, S. Miyata, A. Nishikata, Z. Siroma, Y. Uchimoto, K. Yasuda, K.-i. Kimijima, N. Iwashita, Chem. Rev. 107 (2007) 3904–3951.
[18] S. Bose, T. Kuila, T.X.H. Nguyen, N.H. Kim, K.-t. Lau, J.H. Lee, Prog. Polym. Sci. 36 (2011) 813–843.
[19] J. Mader, L. Xiao, T. Schmidt, B. Benicewicz, in: G.G. Scherer (Ed.), Fuel Cells II, Springer, Berlin Heidelberg, 2008, pp. 63–124.
[20] J. Zhang, Z. Xie, J. Zhang, Y. Tang, C. Song, T. Navessin, Z. Shi, D. Song, H. Wang, D.P. Wilkinson, Z.-S. Liu, S. Holdcroft, J. Power Sources 160 (2006) 872–891.
[21] H.J. Davis, N.W. Thomas, in, Celanese Corporation, New York, NY, 1977.
[22] H. Xu, K. Chen, X. Guo, J. Fang, J. Yin, J. Membr. Sci. 288 (2007) 255–260.
[23] K.Y. Wang, Y. Xiao, T.-S. Chung, Chem. Eng. Sci. 61 (2006) 5807–5817.
[24] Q. Li, C. Pan, J.O. Jensen, P. Noyé, N.J. Bjerrum, Chem. Mater. 19 (2007) 350–352.
[25] P. Noyé, Q. Li, C. Pan, N.J. Bjerrum, Polym. Adv. Technol. 19 (2008) 1270–1275.
[26] J. Senger, I. Yilgor, J. McGrath, R. Patsiga, J. Appl. Polym. Sci. 38 (1989) 373–382.
[27] V. Giménez, A. Mantecón, V. Cádiz, J. Polym. Sci. A Polym. Chem. 34 (1996) 925–934.
[28] S. Wang, C. Zhao, W. Ma, G. Zhang, Z. Liu, J. Ni, M. Li, N. Zhang, H. Na, J. Membr. Sci. 411–412 (2012) 54–63.
[29] M. Han, G. Zhang, Z. Liu, S. Wang, M. Li, J. Zhu, H. Li, Y. Zhang, C.M. Lew, H. Na, J. Mater. Chem. 21 (2011) 2187–2193.
[30] S. Wang, G. Zhang, M. Han, H. Li, Y. Zhang, J. Ni, W. Ma, M. Li, J. Wang, Z. Liu, L. Zhang, H. Na, Int. J. Hydrogen Energy 36 (2011) 8412–8421.
[31] H.-L. Lin, Y.-C. Chou, T.L. Yu, S.-W. Lai, Int. J. Hydrogen Energy 37 (2012) 383–392.
[32] J.-K. Kim, K. Taki, S. Nagamine, M. Ohshima, J. Appl. Polym. Sci. 111 (2009) 2518–2526.
[33] D. Aili, L.N. Cleemann, Q. Li, J.O. Jensen, E. Christensen, N.J. Bjerrum, J. Mater. Chem. 22 (2012) 5444–5453.
[34] H. Vogel, C.S. Marvel, J. Polym. Sci. A Polym. Chem. 34 (1961) 1125–1153.
[35] J.K. Gillham, Science 139 (1963) 494–495.
[36] S. Bhadra, C. Ranganathaiah, N.H. Kim, S.-I. Kim, J.H. Lee, J. Appl. Polym. Sci. 121 (2011) 923–929.
[37] T.-H. Young, J.-H. Huang, W.-Y. Chuang, Eur. Polym. J. 38 (2002) 63–72.
[38] H. Matsuyama, M.-m. Kim, D.R. Lloyd, J. Membr. Sci. 204 (2002) 413–419.
[39] H. Pu, W.H. Meyer, G. Wegner, J. Polym. Sci. B Polym. Phys. 40 (2002) 663–669.
[40] B. Vollmert, Polymer Chemistry, Springer, 1973.
[41] M.P. Stevens, Polymer Chemistry – An Introduction, third ed., Oxford University Press, New York, 1999.
[42] A.Y. Leykin, A.A. Askadskii, V.G. Vasilev, A.L. Rusanov, J. Membr. Sci. 347 (2010) 69–74.
[43] S. Matar, A. Higier, H. Liu, J. Power Sources 195 (2010) 181–184.

Glossary

BOL: begin-of-life
DMAc: dimethylacetamide
ECA: electrochemical surface area
HT-PEMFC: high temperature polymer electrolyte membrane fuel cell
HTPEM: high temperature polymer electrolyte membrane
MEA: membrane electrode assembly
PBI: polybenzimidazole
TGA: thermo gravimetric analysis
XRD: X-ray diffraction